SCIENCE CHINA
Information Sciences

• RESEARCH PAPER •

March 2024, Vol. 67, Iss. 3, 132204:1–132204:15
https://doi.org/10.1007/s11432-023-3886-8

Event-triggered sliding mode control of linear repetitive processes and its application in metal rolling process

Xinyu LV[1], Yugang NIU[1*] & James LAM[2*]

[1]*Key Laboratory of Smart Manufacturing in Energy Chemical Process* (*East China University of Science and Technology*), *Ministry of Education, Shanghai* 200237, *China;*
[2]*Department of Mechanical Engineering, The University of Hong Kong, Hong Kong* 999077, *China*

Received 10 February 2023/Revised 15 June 2023/Accepted 25 July 2023/Published online 26 February 2024

Abstract This paper investigates the design problem of a sliding mode controller for linear repetitive processes (LRPs) with a finite pass length on each pass. Under limited communication resources, an event-triggered mechanism is implemented from the sensors to the controller, whose triggered sequence is consistent with the evolution direction of LRPs. To periodically orchestrate communication between the controller and actuator, a round-robin scheduling mechanism is established based on the pass length. A sliding function involving the state and pass profile is constructed, and the sliding mode controller is designed using triggered states and pass profile signals. Feasible controller gains are attained to ensure the stability of the resultant closed-loop system. Finally, the proposed strategy is implemented for a multi-roll metal rolling process.

Keywords event-triggered mechanism, linear repetitive processes, metal rolling process, round-robin scheduling, sliding mode control

1 Introduction

Linear repetitive processes (LRPs), also known as the multipass processes, consist of a series of sweeps (i.e., passes) defined over a finite duration (i.e., pass length). The output of each pass, termed as pass profile, acts as a forcing function on the next pass. This means that the state of LRPs evolves along the pass over a finite pass length and the pass profile propagates from pass to pass. This makes LRPs exhibit two-directional features. Some representative examples of LRPs include iterative learning control systems [1], metal rolling operations [2], and long-wall coal mining [3]. Owing to their inherent two-dimensional (2D) systems structure, the conventional one-dimensional (1D) control systems theory cannot be directly applied to LRPs. Hence, an effective method is to transform LRPs into their equivalent 2D state-space model (e.g., Roesser model or Fornasini-Marchesini model), by which the relevant control design and analysis may be made. However, some key properties (e.g., pass profile controllability) for LRPs cannot be reflected by the 2D state-space model (see [3–6]). Instead, Paszke et al. [7] directly analyzed the stability along the pass of LRPs not transformed to the 2D state-space model, where the controller was constructed as a linear combination of the current pass state and previous pass profile. The Hankel-type performance for differential and discrete LRPs was analyzed in [8] by achieving stability along the pass process.

In a typical networked control system, information among various components is transmitted through a shared network with limited bandwidth. In particular, for LRPs, both the direction signals (state and pass profile) would be transmitted over the network. Such resource-sharing features inevitably led to unnecessary signal transmission and communication burdens. An effective way of improving the efficient usage of network resources is to introduce an event-triggered (ET) mechanism for reducing the frequency of data transmission. A growing body of literature has investigated the ET control issues for 1D systems (e.g., [9–12]) and 2D systems (e.g., [13–16]). Accordingly, the ET cost-guaranteed control problem was

* Corresponding author (email: acniuyg@ecust.edu.cn, james.lam@hku.hk)

addressed in [15] via converting LRPs into a 2D state-space model. Another effective way of mitigating data congestion is to schedule the transmission order of the controller/sensor via several communication protocols, such as the round-robin (RR) protocol and the most commonly used periodic protocol. The primary function of the RR protocol is to grant equitable privileges to each system component to transmit signals over the network one by one in a cyclic manner (see [17–20]). The RR protocol was adopted in [20] to periodically orchestrate the communication between sensors and filter for time-varying LRPs, where the LRPs were transformed into a 2D state-space model.

In practical applications, parameter uncertainties and external disturbances are common and inevitably impair system performance. Sliding mode control (SMC) has been widely applied in a variety of systems because it can offer efficient solutions for resolving such two issues, see [21–25] for 1D systems and [16, 26] for 2D systems. Moreover, some ET schemes (e.g., [27–30]) and RR scheduling protocols (e.g., [18, 31]) have been presented via SMC methods to reduce communication load and attenuate the effect of uncertainties and disturbances simultaneously. Recently, a preliminary finding was published on the observer-based SMC scheme for differential LRPs in [32], where two direction-independent sliding functions and sliding mode controllers were designed, respectively, for pass-to-pass and pass directions under ideal communication case without bandwidth constraints. However, investigating the SMC problem of LRPs with constrained communication resources is extremely important from both theoretical and practical perspectives. To this end, several essential questions had to be answered: (a) How to implement the ET mechanism and RR protocol following the evolution feature of LRPs? (b) Does the pass length affect the ET mechanism and the scheduling rule? (c) How to design a feasible sliding mode controller under the ET strategy and RR protocols? These issues are crucial and serve as an inspiration for the current investigation.

In this work, we intend to address the design problem of ET sliding mode controller for LRPs under channel scheduling. According to the state and evolution direction of LRPs, an ET mechanism is developed to govern the transmission of both the state and pass profile signals from the sensors to the controller (S/C). Afterward, an RR protocol is employed to periodically schedule the communication from the controller to the actuator (C/A), and only one controller node is selected to deliver its signal to the appropriate actuator node. Then, the stability of the closed-loop system is analyzed and the corresponding sufficient conditions are derived. Finally, the provided control strategy is applied to the multi-roll metal rolling process. The following is a list of this paper's main contributions.

(1) Different from [15], an ET mechanism is designed by directly analyzing LRPs and only using its state signal, under which the triggering sequence as a two-indicator sequence is not only consistent with the evolution direction of LRPs, but also reflects the 2D evolution characteristics of signals.

(2) Compared with [17, 20], an RR scheduling rule that is dependent on pass length is defined by utilizing the inherent time sequence of LRPs. Under this rule, the controller node is selected one by one to transmit its signal to the actuator.

(3) An ET sliding mode controller is designed via the current triggered state and previous pass profile, which reveals a switched-like feature; that is, the controller gains are different according to the triggered location and pass. The feature of this controller sets it apart from previous studies, e.g., [14] on 2D systems and [32] on LRPs.

(4) The relationship between the current pass profile and the pass profile at the latest triggered point is established, which is beneficial for loosening the restrictions on system stability conditions.

Notations. The set of positive integers is $\mathbb{Z}^+$, while the set of all integers from a to b is $\mathbb{Z}_a^b$. The modulo function $\mathrm{mod}(a, b)$ represents the unique nonnegative remainder on division of the integer a by the positive integer b. The symbol $\mathrm{diag}\{A_1, A_2\}$ represents a block-diagonal matrix made up of the matrices A_1 and A_2. $\|\cdot\|$ stands for the induced matrix 2-norm. The term induced by symmetry is indicated in a matrix by "$*$". If $Y > 0$ (or $Y < 0$) for a real symmetric matrix, then Y is a positive (or negative) definite matrix. The maximal (minimal) eigenvalue of matrix Y is represented by the values $\lambda_{\max}(Y)$ ($\lambda_{\min}(Y)$). Matrix dimensions are presumed to be compatible unless otherwise stated.

2 Problem formulation and preliminaries

The basic principle of LRPs is to finish the task for the current pass before moving to the next pass, where each pass executes a limited number of tasks. Such a physical process is usually described in two dimensions (namely, the dimension p along the pass direction and the dimension k along the pass-to-pass

direction) and modeled by

$$\begin{cases} x_{k+1}(p+1) = A_p x_{k+1}(p) + B_0 y_k(p) + B(u_{k+1}(p) + f(x_{k+1}(p), y_k(p))), \\ y_{k+1}(p) = C x_{k+1}(p) + D_0 y_k(p) + D u_{k+1}(p), \end{cases} \tag{1}$$

where $k \in \mathbb{Z}^+$, $p \in \mathbb{Z}_0^{N-1}$ with N denoting the length of each pass; $x_{k+1}(p) \in \mathbb{R}^n$ and $y_{k+1}(p) \in \mathbb{R}^s$ are, respectively, the states and pass profile at the location p on the $(k+1)$-th pass; $u_{k+1}(p) \in \mathbb{R}^m$ is the actuator input signal on the $(k+1)$-th pass and the corresponding control signal is defined as $v_{k+1}(p)$ with $u_{k+1}(p) \triangleq [u_{k+1}^1(p)\ u_{k+1}^2(p)\ \cdots\ u_{k+1}^m(p)]^{\mathrm{T}}$ and $v_{k+1}(p) \triangleq [v_{k+1}^1(p)\ v_{k+1}^2(p)\ \cdots\ v_{k+1}^m(p)]^{\mathrm{T}}$; $f(x_{k+1}(p), y_k(p))$ is the external disturbance satisfying $\|f(x_{k+1}(p), y_k(p))\|^2 \leqslant f_1^2\|x_{k+1}(p)\|^2 + f_2^2\|y_k(p)\|^2$ with known constants $f_1, f_2 > 0$; A_p is composed of the known matrix A and parameter uncertainties $\Delta A(p)$ (i.e., $A_p = A + \Delta A(p)$) and $\Delta A(p)$ satisfies $\Delta A(p) = E\Gamma(p)H$, $\Gamma^{\mathrm{T}}(p)\Gamma(p) < I$ with E and H being known matrices; B, C, D, B_0, and D_0 are known matrices.

Remark 1. It is noted from model (1) that the next state $x_{k+1}(p+1)$ at the $(k+1)$-th pass depends on the current state $x_{k+1}(p)$ and input $u_{k+1}(p)$ at the same pass, and the pass profile $y_k(p)$ at the previous k-th pass. In other words, the evolution of states in LRPs depends on two directional signals, i.e., the signal along the pass and the signal along the pass-to-pass, which reflects the 2D characteristic of LRPs. Besides, the presence of the pass profile $y_k(p)$ embodies the main difference between LRPs and 2D state-space models.

The boundary conditions, i.e., the initial values of states on each pass and initial pass profile on the 0-th pass, are specified as

$$x_{k+1}(0) = d_{k+1},\ y_0(p) = e(p),\ \text{for } k \geqslant 0, 0 \leqslant p \leqslant N \tag{2}$$

with $d_{k+1} \in \mathbb{R}^n$ being the known constant vector and $e(p) \in \mathbb{R}^q$ being the known function vector.

In this work, we give the stability definition based on Lyapunov stability theory.

Definition 1 ([33])**.** For LRPs (1), one introduces the Lyapunov functional $V(k,p) = V_1(k,p) + V_2(k,p)$ with $V_1(k,p) = x_{k+1}^{\mathrm{T}}(p)Px_{k+1}(p)$ and $V_2(k,p) = y_k^{\mathrm{T}}(p)Qy_k(p)$, where P and Q are positive definite matrices to be found. If $\Delta V(k,p) = V_1(k,p+1) - V_1(k,p) + V_2(k+1,p) - V_2(k,p) < 0$, LRPs (1) are stable along the pass.

In order to achieve the stability of LRPs (1), we can construct a sliding function as

$$s_{k+1}(p) = G_1 x_{k+1}(p) + G_2 y_{k+1}(p-1), \tag{3}$$

where G_1 and G_2 are the designing matrices. Apparently, the sliding variable $s_{k+1}(p)$ reveals a significant correlation with the state $x_{k+1}(p)$ and pass profile $y_{k+1}(p-1)$, which displays bidirectional characteristics of the sliding variables.

Furthermore, we can design SMC law $v_{k+1}(p)$ as

$$v_{k+1}(p) = K_1 x_{k+1}(p) + K_2 y_k(p) - \rho_{k+1}(p)\mathrm{sign}(s_{k+1}(p)), \tag{4}$$

where K_1 and K_2 are the designing matrices and $\rho_{k+1}(p)$ is the robustness term given as

$$\rho_{k+1}(p) = \sqrt{f_1^2\|x_{k+1}(p)\|^2 + f_2^2\|y_k(p)\|^2}.$$

It is important to note that the control law (4) takes into account both the present state and the prior pass profile, both of which are available for the controller under the ideal network conditions. However, as discussed in Section 1, the information transmission via shared-networks may lead to congestion and packet-loss, due to the burden of unnecessary communications.

To reduce the number of transmitted signals and avoid data congestion, an event trigger will be introduced in this work to determine the transmission of both the state and pass profile signals in the S/C channel, and an RR scheduling protocol will be utilized to regulate the access of controller nodes to the network. As shown in Figure 1, once an event occurs, the state and pass profile signals will be transmitted to the controller side. Meanwhile, this pass profile signal will be stored in the Buffer and the previously transmitted pass profile signal will be taken from the Buffer to compute the current control signal. Moreover, under the RR scheduling protocol, only one controller node will be chosen to send its signal at each moment.

In the subsequent sections, we shall propose an ET scheme, under which the designed SMC law (4) can ensure the stability along the pass of the LRPs (1) under the RR protocol.

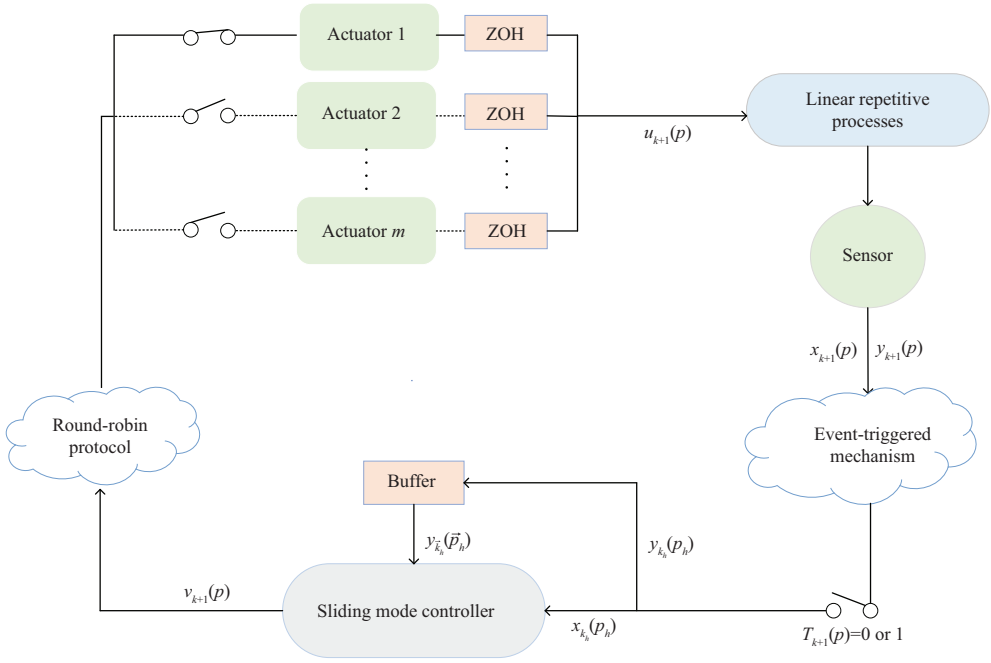

Figure 1 (Color online) Communication scheme for LRPs.

3 Sliding mode control under limited communication

3.1 Event-triggered SMC scheme

Considering the structural property of LRPs (1), its evolution direction is unique as follows:

$$(1,0) < \cdots < (1,N) < (2,0) < \cdots < (2,N) < \cdots, \tag{5}$$

where point (k,p) denotes the location p on the k-th pass. For any two points (k_1,p_1) and (k_2,p_2), the relation, $(k_2,p_2) > (k_1,p_1)$, means $(k_2,p_2) \in \mathcal{S}_1 \cup \mathcal{S}_2$ with $\mathcal{S}_1 \triangleq \{(k,p) \mid k = k_1, p > p_1\}$ and $\mathcal{S}_2 \triangleq \{(k,p) \mid k > k_1, p \in [0,N]\}$. That is, the set $\mathcal{S}_1$ prescribes different points on the same pass k, which depends on the p value. The other set $\mathcal{S}_2$ prescribes different points on the different passes.

Thus, when the signal transmission is determined by an event, the triggered sequence is a subsequence of the above sequence (5) and defined as

$$(1,0) = (k_0,p_0) < (k_1,p_1) < \cdots < (k_h,p_h) < \cdots, \tag{6}$$

where (k_h,p_h) stands for the h-th triggered point with the location p_h on the k_h-th pass.

In this work, the triggered sequence (6) is determined by the following triggering condition:

$$(k_{h+1},p_{h+1}) \triangleq \min_{(k+1,p)>(k_h,p_h)} \{(k+1,p) \mid e_{k+1}^{\mathrm{T}}(p)\Omega e_{k+1}(p) > \theta x_{k+1}^{\mathrm{T}}(p)\Omega x_{k+1}(p)\}, \tag{7}$$

where $e_{k+1}(p) \triangleq x_{k+1}(p) - x_{k_h}(p_h)$ represents the difference between the current state signal $x_{k+1}(p)$ and the last transmitted state signal $x_{k_h}(p_h)$, $\theta \in [0,1)$ is the given threshold, and the weighted matrix Ω will be designed later.

Once an event occurs, both state signal $x_{k+1}(p)$ and pass profile signal $y_{k+1}(p)$ at point $(k+1,p)$ are transmitted to the controller side. As stated under expression (4), the controller (4) depends on state signal $x_{k+1}(p)$ on the $(k+1)$-th pass and pass profile signal $y_k(p)$ on the k-th pass. As such, the pass profile signal $y_{k+1}(p)$ will be stored in the Buffer at the controller side and utilized to calculate the controller signal on the next pass. It is known that the controller will not receive the current state and pass profile signals if the ET condition (7) is not satisfied. To solve this problem, the latest triggered signals will be utilized to compensate the untransmitted signals, that is, the available state signal $\bar{x}_{k+1}(p)$ and pass profile signal $\bar{y}_{k+1}(p)$ for the controller at the point $(k+1,p)$ are, respectively, given as

$$\bar{x}_{k+1}(p) = \begin{cases} x_{k+1}(p), & \text{if } T_{k+1}(p) = 1, \\ x_{k_h}(p_h), & \text{if } T_{k+1}(p) = 0, \end{cases} \tag{8}$$

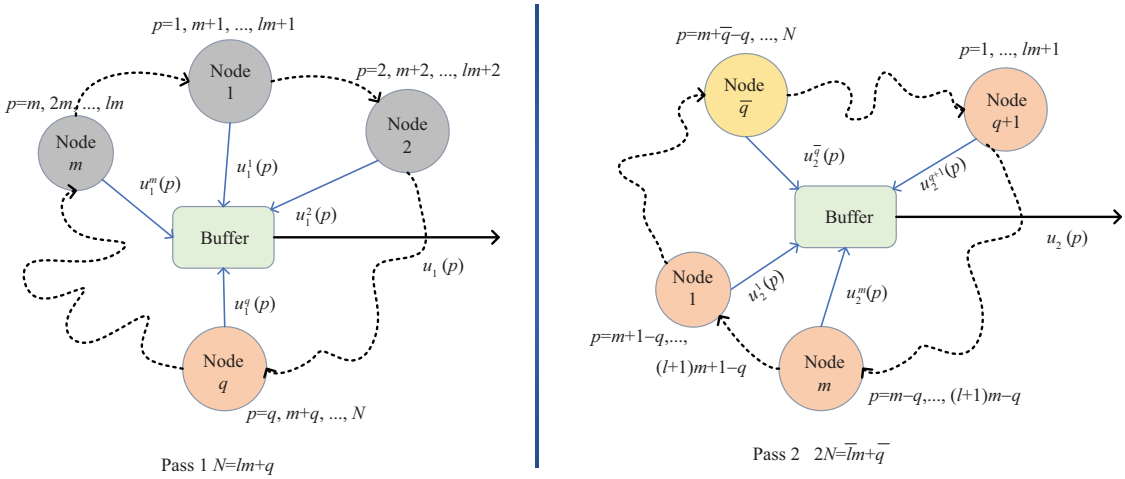

Figure 2 (Color online) RR scheduling cases for LRPs.

and

$$\bar{y}_{k+1}(p) = \begin{cases} y_{k+1}(p), & \text{if } T_{k+1}(p) = 1, \\ y_{k_h}(p_h), & \text{if } T_{k+1}(p) = 0, \end{cases} \tag{9}$$

where $T_{k+1}(p) = 1$ denotes that the ET condition (7) is satisfied at the point $(k+1, p)$, that is, state $x_{k+1}(p)$ and pass profile $y_{k+1}(p)$ will be transmitted to the controller side; and $T_{k+1}(p) = 0$ means that no event is triggered and the last transmitted signals $x_{k_h}(p_h)$ and $y_{k_h}(p_h)$ will be used for the controller.

Accordingly, under the ET scheme (7) and compensating strategy (8) and (9), the SMC law (4) is modified as

$$v_{k+1}(p) = K_1 \bar{x}_{k+1}(p) + K_2 \bar{y}_k(p) - \bar{\rho}_{k+1}(p)\text{sign}(\bar{s}_{k+1}(p)), \tag{10}$$

which, for $(k+1, p) \in [(k_h, p_h), (k_{h+1}, p_{h+1}))$, is equivalent to

$$v_{k+1}(p) = K_1 x_{k_h}(p_h) + K_2 y_{\vec{k}_h}(\vec{p}_h) - \rho_{k_h}(p_h)\text{sign}(s_{k_h}(p_h)), \tag{11}$$

where $y_{\vec{k}_h}(\vec{p}_h)$ is the pass profile at the latest triggered point $(\vec{k}_h, \vec{p}_h)$ of point (k, p), $s_{k_h}(p_h)$ is the sliding variable $s_{k+1}(p)$ in (3) with $x_{k+1}(p)$ and $y_{k+1}(p-1)$ replaced by the triggered state and pass profile signals, and the robustness term is modified as $\rho_{k_h}(p_h) = \sqrt{f_1^2 \|x_{k_h}(p_h)\|^2 + f_2^2 \|y_{\vec{k}_h}(\vec{p}_h)\|^2}$.

Besides, it should be noted that there are $N+1$ points between points (k, p) and $(k+1, p)$; therefore, there may be none or several triggering intervals between the two points, i.e, $(\vec{k}_h, \vec{p}_h) \leqslant (k_h, p_h)$.

3.2 Round-robin scheduling scheme

In this work, the RR protocol is utilized to assign the usage privilege of controller nodes to the communication network in a cyclic way, that is, each controller node is selected in turn to transmit its signal to the corresponding actuator node. It is worthy of pointing out that at each point (k, p), only one controller node $v_k^\iota(p)$, $\iota \in \{1, 2, \ldots, m\}$ is selected according to the scheduling rule of RR protocol. Let $\sigma_k(p) \in \{1, 2, \ldots, m\}$ (termed as the token) represent the selected controller node, which is determined via the following rule:

$$\sigma_k(p) = \text{mod}((k-1)N + p - 1, m) + 1. \tag{12}$$

Apparently, the token $\sigma_k(p)$ is dependent on location p and pass number k. As an example, Figure 2 shows the tokens of the first two passes.

Remark 2. In this work, the ordering of the given token is the same as that of LRPs evolution (the ordering in (5)); i.e., the controller node is selected periodically at each pass and pass to pass.

According to the scheduling rule (12), at each point (k,p), except for the controller node with the token $\sigma_k(p)$, other nodes cannot transmit their signals; that is, their corresponding actuator nodes do not receive any signals. As a means of dealing with the above issues, in this work, the actuator may utilize previously received signals for those untransmitted controller nodes. That is, the actuator signal $u_k^\iota(p), \iota \in \{1,\ldots,m\}$ is given as

$$u_k^\iota(p) = \begin{cases} v_k^\iota(p), & \sigma_k(p) = \iota, \\ u_k^\iota(p-1), & \text{otherwise.} \end{cases} \tag{13}$$

This means that the actuator signal $u_k(p)$ at the plant side can be expressed as

$$u_k(p) = \Phi_{\sigma_k(p)} v_k(p) + (I - \Phi_{\sigma_k(p)}) u_k(p-1) \tag{14}$$

with $\Phi_{\sigma_k(p)} \triangleq \mathrm{diag}\{\delta(\sigma_k(p),1),\ldots,\delta(\sigma_k(p),m)\}$, $\delta(\sigma_k(p),\iota) \triangleq \delta(\sigma_k(p)-\iota) = 1$ for $\sigma_k(p) = \iota$, otherwise, $\delta(\sigma_k(p)-\iota) = 0$. Here, we specify $u_k(0) = 0$ for $k \geqslant 0$.

Then, by combining the communication situation at S/C and C/A sides, the closed-loop system composed of model (1) and controller (11) is described as

$$\begin{cases} x_{k+1}(p+1) = (A+\Delta A(p)+B\Phi_{\sigma_{k+1}(p)}K_1)x_{k+1}(p)+B\Phi_{\sigma_{k+1}(p)}K_1 e_{k+1}(p)+Bf(x_{k+1}(p),y_k(p))+B_0 y_k(p) \\ \qquad\qquad +B\Phi_{\sigma_{k+1}(p)}K_2 y_{\vec{k}_h}(\vec{p}_h)-B\Phi_{\sigma_{k+1}(p)}\rho_{k_h}(p_h)\mathrm{sign}(s_{k_h}(p_h))+B(I-\Phi_{\sigma_{k+1}(p)})u_{k+1}(p-1), \\ y_{k+1}(p) = (C+D\Phi_{\sigma_{k+1}(p)}K_1)x_{k+1}(p)+D_0 y_k(p)-D\Phi_{\sigma_{k+1}(p)}K_1 e_{k+1}(p)+D\Phi_{\sigma_{k+1}(p)}K_2 y_{\vec{k}_h}(\vec{p}_h) \\ \qquad\qquad -D\Phi_{\sigma_{k+1}(p)}\rho_{k_h}(p_h)\mathrm{sign}(s_{k_h}(p_h))+D(I-\Phi_{\sigma_{k+1}(p)})u_{k+1}(p-1). \end{cases} \tag{15}$$

It is noted that the pass profiles $y_k(p)$ and $y_{\vec{k}_h}(\vec{p}_h)$ are present simultaneously in expression (15). Thus, for analyzing the stability of the closed-loop system (15), a conventional and direct method would integrate the two terms $y_k^{\mathrm{T}}(p)Qy_k(p)$ and $y_{\vec{k}_h}^{\mathrm{T}}(\vec{p}_h)Qy_{\vec{k}_h}(\vec{p}_h)$ into the constructed Lyapunov functional. Yet, such a method cannot be applied in the current situation because it is hard to give the dynamic equation of pass profile $y_{\vec{k}_h}(\vec{p}_h)$. Therefore, to avoid the shortcoming related to $y_{\vec{k}_h}(\vec{p}_h)$, we first establish the relationships between $y_k(p)$ and $y_{\vec{k}_h}(\vec{p}_h)$ in the following lemma.

Lemma 1. For any two pass profiles $y_k(p)$ and $y_{\bar{k}}(\bar{p})$, the difference $y_k(p) - y_{\bar{k}}(\bar{p})$ is given as

$$0, \qquad \text{if } k = \bar{k},\ p = \bar{p}, \tag{16a}$$

$$\sum_{j=\bar{p}}^{p-1}(y_k(j+1) - y_{\bar{k}}(j)), \qquad \text{if } k = \bar{k},\ p > \bar{p}, \tag{16b}$$

$$\sum_{i=\bar{k}}^{k-1}(y_{i+1}(p) - y_i(\bar{p})), \qquad \text{if } k > \bar{k},\ p = \bar{p}, \tag{16c}$$

$$\sum_{i=\bar{k}}^{k-1}(y_{i+1}(p) - y_i(\bar{p})) + \sum_{j=\bar{p}}^{p-1}(y_k(j+1) - y_{\bar{k}}(j)), \quad \text{otherwise.} \tag{16d}$$

Proof. The above equalities can be attained readily by calculating.

Using the relations in Lemma 1, the pass profile $y_{\vec{k}_h}(\vec{p}_h)$ is unnecessarily included in the Lyapunov functional (see the proof procedure in Theorem 1 later) such that the dimension of the Lyapunov functional may be decreased. Besides, it is also unnecessary to provide a bound on the term $y_{\vec{k}_h}(\vec{p}_h)$. As such, the restrictions on system stability conditions are loosened in some extent.

4 Performance analysis

In this section, we shall analyze the stability of the closed-loop system (15) and the reachability of the specified sliding surface $s_{k+1}(p) = 0$. To facilitate subsequent developments, first let $\iota \triangleq \sigma_{k+1}(p)$ and $\bar{\iota} \triangleq \sigma_{k+1}(p+1)$. Apparently, one has $\bar{\iota} = \iota + 1$ for $1 \leqslant \iota < m$, and $\bar{\iota} = 1$ for $\iota = m$.

Theorem 1. The closed-loop system (15) is stable along the pass under the ET scheme (7) and RR protocol (12), if there exist matrices $P_{1,\iota}>0$, $P_{2,\iota}>0$, $P_{3,\iota}>0$, $\Omega>0$, $Y_\iota=Y_\iota^{\mathrm{T}}$, K_1, K_2, and positive scalars $\epsilon_{1,\iota}$, $\epsilon_{2,\iota}$ satisfying (for $\iota,\bar{\iota}=1,2,\ldots,m$)

$$\Pi_{1,\iota}\triangleq\Pi_{11,\iota}+\Gamma_{1,\iota}^{\mathrm{T}}P_{1,\bar{\iota}}\Gamma_{1,\iota}+\Gamma_{2,\iota}^{\mathrm{T}}P_{2,\bar{\iota}}\Gamma_{2,\iota}+\Gamma_{3,\iota}^{\mathrm{T}}P_{3,\bar{\iota}}\Gamma_{3,\iota}<0, \tag{17}$$

for $k>\vec{k}_h$ and $p>\vec{p}_h$,

$$\bar{\Pi}_{1,\iota}\triangleq\bar{\Pi}_{11,\iota}+\bar{\Gamma}_{1,\iota}^{\mathrm{T}}P_{1,\bar{\iota}}\bar{\Gamma}_{1,\iota}+\bar{\Gamma}_{2,\iota}^{\mathrm{T}}P_{2,\bar{\iota}}\bar{\Gamma}_{2,\iota}+\bar{\Gamma}_{3,\iota}^{\mathrm{T}}P_{3,\bar{\iota}}\bar{\Gamma}_{3,\iota}<0, \tag{18}$$

for $k=\vec{k}_h$ and $p>\vec{p}_h$ or $k>\vec{k}_h$ and $p=\vec{p}_h$, and

$$\check{\Pi}_{1,\iota}\triangleq\check{\Pi}_{11,\iota}+\check{\Gamma}_{1,\iota}^{\mathrm{T}}P_{1,\bar{\iota}}\check{\Gamma}_{1,\iota}+\check{\Gamma}_{2,\iota}^{\mathrm{T}}P_{2,\bar{\iota}}\check{\Gamma}_{2,\iota}+\check{\Gamma}_{3,\iota}^{\mathrm{T}}P_{3,\bar{\iota}}\check{\Gamma}_{3,\iota}<0, \tag{19}$$

for $k=\vec{k}_h$ and $p=\vec{p}_h$, where

$$\bar{\Pi}_{11,\iota}\triangleq\begin{bmatrix}\Psi_1 & \Psi_2\\ * & -Y_\iota\end{bmatrix},\Pi_{11,\iota}\triangleq\begin{bmatrix}\Psi_1 & \Psi_2 & \Psi_2\\ * & -Y_\iota & -Y_\iota\\ * & * & -Y_\iota\end{bmatrix},\check{\Pi}_{11,\iota}\triangleq\begin{bmatrix}\Psi_{11} & \Psi_{12} & 0 & 0\\ * & \Psi_{22} & 0 & 0\\ * & * & \check{\Psi}_{33} & 0\\ * & * & * & \Psi_{55}\end{bmatrix},\Psi_1\triangleq\begin{bmatrix}\Psi_{11} & \Psi_{12} & 0 & 0 & 0\\ * & \Psi_{22} & 0 & 0 & 0\\ * & * & \Psi_{33} & \frac{Y_\iota}{2} & 0\\ * & * & * & \Psi_{44} & 0\\ * & * & * & * & \Psi_{55}\end{bmatrix},$$

$$\Psi_2\triangleq\begin{bmatrix}0 & 0 & \dfrac{Y_\iota}{2} & -Y_\iota & 0\end{bmatrix}^{\mathrm{T}},\Psi_{11}\triangleq-P_{1,\iota}+\theta\Omega+(\epsilon_{1,\iota}+\epsilon_{2,\iota}m)f_1^2I,\Psi_{22}\triangleq-\Omega+\epsilon_{2,\iota}mf_1^2I,\Psi_{12}\triangleq-2\epsilon_{2,\iota}mf_1^2I,$$

$$\Psi_{33}\triangleq-P_{3,\iota}+\epsilon_{1,\iota}f_2^2I,\check{\Psi}_{33}\triangleq\Psi_{33}+\epsilon_{2,\iota}mf_2^2I,\Psi_{44}\triangleq-Y_\iota+\epsilon_{2,\iota}mf_2^2I,\Psi_{55}\triangleq\mathrm{diag}\{-P_{2,\iota},-\epsilon_{1,\iota}I,-\epsilon_{2,\iota}I\},$$

$$\bar{A}\triangleq A+\Delta A(p)+B\Phi_\iota K_1,\hat{\Gamma}_{1,\iota}\triangleq[\bar{A}\ -B\Phi_\iota K_1\ B_0\ B\Phi_\iota K_2\ B(I-\Phi_\iota)\ B\ -B\Phi_\iota],\bar{\Gamma}_{q,\iota}\triangleq[\hat{\Gamma}_{q,\iota}\ 0],$$

$$\check{\Gamma}_{1,\iota}\triangleq[\bar{A}\ -B\Phi_\iota K_1\ B_0+B\Phi_\iota K_2\ B(I-\Phi_\iota)\ B\ -B\Phi_\iota],\hat{\Gamma}_{2,\iota}\triangleq[\Phi_\iota K_1\ -\Phi_\iota K_1\ 0\ \Phi_\iota K_2\ I-\Phi_\iota\ 0\ -\Phi_\iota],$$

$$\check{\Gamma}_{2,\iota}\triangleq[\Phi_\iota K_1\ -\Phi_\iota K_1\ \Phi_\iota K_2\ I-\Phi_\iota\ 0\ -\Phi_\iota],\hat{\Gamma}_{3,\iota}\triangleq[C+D\Phi_\iota K_1\ -D\Phi_\iota K_1\ D_0\ D\Phi_\iota K_2\ D(I-\Phi_\iota)\ 0\ -D\Phi_\iota],$$

$$\check{\Gamma}_{3,\iota}\triangleq[C+D\Phi_\iota K_1\ -D\Phi_\iota K_1\ D_0+D\Phi_\iota K_2\ D(I-\Phi_\iota)\ 0\ -D\Phi_\iota],\Gamma_{q,\iota}\triangleq[\hat{\Gamma}_{q,\iota}\ 0\ 0],q=1,2,3.$$

Proof. Select the following Lyapunov functional:

$$V(k,p,\iota)=V_1(k+1,p,\iota)+V_2(k,p,\iota) \tag{20}$$

with $V_1(k+1,p,\iota)\triangleq x_{k+1}^{\mathrm{T}}(p)P_{1,\iota}x_{k+1}(p)+u_{k+1}^{\mathrm{T}}(p-1)P_{2,\iota}u_{k+1}(p-1)$ and $V_2(k,p,\iota)\triangleq y_k^{\mathrm{T}}(p)P_{3,\iota}y_k(p)$.

We first define the differences $\Delta V(k,p,\iota)$, $\Delta V_1(k,p,\iota)$, and $\Delta V_2(k,p,\iota)$ as

$$\Delta V(k,p,\iota)\triangleq\Delta V_1(k,p,\iota)+\Delta V_2(k,p,\iota), \tag{21}$$

$$\begin{aligned}\Delta V_1(k,p,\iota)\triangleq{}&x_{k+1}^{\mathrm{T}}(p+1)P_{1,\bar{\iota}}x_{k+1}(p+1)+u_{k+1}^{\mathrm{T}}(p)P_{2,\bar{\iota}}u_{k+1}(p)\\&-x_{k+1}^{\mathrm{T}}(p)P_{1,\iota}x_{k+1}(p)-u_{k+1}^{\mathrm{T}}(p-1)P_{2,\iota}u_{k+1}(p-1),\end{aligned} \tag{22}$$

$$\Delta V_2(k,p,\iota)\triangleq y_{k+1}^{\mathrm{T}}(p)P_{3,\bar{\iota}}y_{k+1}(p)-y_k^{\mathrm{T}}(p)P_{3,\iota}y_k(p). \tag{23}$$

According to (11) and (14), we have

$$\begin{aligned}u_{k+1}(p)&=\Phi_{\sigma_{k+1}(p)}v_{k+1}(p)+(I-\Phi_{\sigma_{k+1}(p)})u_{k+1}(p-1)\\&=\Phi_{\sigma_{k+1}(p)}\big(K_1x_{k+1}(p)-K_1e_{k+1}(p)+K_2y_{\vec{k}_h}(\vec{p}_h)-\rho_{k_h}(p_h)\mathrm{sign}(s_{k_h}(p_h))\big)\\&\quad+(I-\Phi_{\sigma_{k+1}(p)})u_{k+1}(p-1).\end{aligned} \tag{24}$$

For difference $\Delta V_1(k,p)$, one has from (15) and (24)

$$\begin{aligned}\Delta V_1(k,p,\iota)=&\zeta_0^{\mathrm{T}}(k,p)\big(\hat{\Gamma}_{1,\iota}^{\mathrm{T}}P_{1,\bar{\iota}}\hat{\Gamma}_{1,\iota}+\hat{\Gamma}_{2,\iota}^{\mathrm{T}}P_{2,\bar{\iota}}\hat{\Gamma}_{2,\iota}\big)\zeta_0(k,p)\\&-x_{k+1}^{\mathrm{T}}(p)P_{1,\iota}x_{k+1}(p)-u_{k+1}^{\mathrm{T}}(p-1)P_{2,\iota}u_{k+1}(p-1)\end{aligned} \tag{25}$$

with $\zeta_0(k,p) \triangleq [x_{k+1}^{\mathrm{T}}(p)\ e_{k+1}^{\mathrm{T}}(p)\ y_k^{\mathrm{T}}(p)\ y_{\vec{k}_h}(\vec{p}_h)\ u_{k+1}^{\mathrm{T}}(p-1)\ f^{\mathrm{T}}(x_{k+1}(p),y_k(p))\ (\rho'_{k_h}(p_h))^{\mathrm{T}}]^{\mathrm{T}}$ and $\rho'_{k_h}(p_h) \triangleq \rho_{k_h}(p_h)\mathrm{sign}(s_{k_h}(p_h))$.

Similarly, we have

$$\Delta V_2(k,p,\iota) = \zeta_0^{\mathrm{T}}(k,p)\hat{\Gamma}_{3,\iota}^{\mathrm{T}}P_{3,\bar{\iota}}\hat{\Gamma}_{3,\iota}\zeta_0(k,p) - y_k^{\mathrm{T}}(p)P_{3,\iota}y_k(p). \tag{26}$$

In what follows, we will introduce some zero terms to handle the terms related to $y_{\vec{k}_h}(\vec{p}_h)$ by utilizing the relationship between the pass profile $y_k(p)$ and $y_{\vec{k}_h}(\vec{p}_h)$ under four different situations.

Case 1: $k > \vec{k}_h$ **and** $p > \vec{p}_h$**.**

In view of relation (16d) in Lemma 1, there exist symmetric matrices Y_ι, $\iota \in \{1,2,\ldots,m\}$ with appropriate dimensions satisfying

$$\begin{aligned}&\left[y_k(p) - y_{\vec{k}_h}(\vec{p}_h) - \sum_{i=\vec{k}_h}^{k-1}(y_{i+1}(\vec{p}_h) - y_i(\vec{p}_h)) - \sum_{j=\vec{p}_h}^{p-1}(y_k(j+1) - y_k(j))\right]^{\mathrm{T}} Y_\iota \\ &\quad\times\left[y_{\vec{k}_h}(\vec{p}_h) + \sum_{i=\vec{k}_h}^{k-1}(y_{i+1}(\vec{p}_h) - y_i(\vec{p}_h)) + \sum_{j=\vec{p}_h}^{p-1}(y_k(j+1) - y_k(j))\right] \equiv 0.\end{aligned} \tag{27}$$

Substituting (22)–(27) into (21) yields

$$\begin{aligned}\Delta V(k,p,\iota) =& \zeta_1^{\mathrm{T}}(k,p)(\Gamma_{1,\iota}^{\mathrm{T}}P_{1,\bar{\iota}}\Gamma_{1,\iota} + \Gamma_{2,\iota}^{\mathrm{T}}P_{2,\bar{\iota}}\Gamma_{2,\iota} + \Gamma_{3,\iota}^{\mathrm{T}}P_{3,\bar{\iota}}\Gamma_{3,\iota})\zeta_1(k,p) + \left[y_k(p) - y_{\vec{k}_h}(\vec{p}_h)\right. \\ &- \sum_{i=\vec{k}_h}^{k-1}(y_{i+1}(\vec{p}_h) - y_i(\vec{p}_h)) - \left.\sum_{j=\vec{p}_h}^{p-1}(y_k(j+1) - y_k(j))\right]^{\mathrm{T}} Y_\iota \left[y_{\vec{k}_h}(\vec{p}_h) + \sum_{i=\vec{k}_h}^{k-1}(y_{i+1}(\vec{p}_h) - y_i(\vec{p}_h))\right. \\ &+ \left.\sum_{j=\vec{p}_h}^{p-1}(y_k(j+1) - y_k(j))\right] - x_{k+1}^{\mathrm{T}}(p)P_{1,\iota}x_{k+1}(p) - y_k^{\mathrm{T}}(p)P_{3,\iota}y_k(p) \\ &- u_{k+1}^{\mathrm{T}}(p-1)P_{2,\iota}u_{k+1}(p-1)\end{aligned} \tag{28}$$

with $\zeta_1(k,p) \triangleq [\zeta_0^{\mathrm{T}}(k,p)\ \ \sum_{i=\vec{k}_h}^{k-1}(y_{i+1}(\vec{p}_h) - y_i(\vec{p}_h))^{\mathrm{T}}\ \ \sum_{j=\vec{p}_h}^{p-1}(y_k(j+1) - y_k(j))^{\mathrm{T}}]^{\mathrm{T}}$.

Noting the relation $\|f(x_{k+1}(p),y_k(p))\|^2 \leqslant f_1^2\|x_{k+1}(p)\|^2 + f_2^2\|y_k(p)\|^2$, one has

$$-\epsilon_{1,\iota}\|f(x_{k+1}(p),y_k(p))\|^2 + \epsilon_{1,\iota}(f_1^2\|x_{k+1}(p)\|^2 + f_2^2\|y_k(p)\|^2) \geqslant 0. \tag{29}$$

Meanwhile, one also has from $\mathrm{sign}(s^{\mathrm{T}}(\cdot))\mathrm{sign}(s(\cdot)) \leqslant m$

$$\begin{aligned}&-\epsilon_{2,\iota}(\rho'_{k_h}(p_h))^{\mathrm{T}}\rho'_{k_h}(p_h) + \epsilon_{2,\iota}m(f_1^2\|x_{k_h}(p_h)\|^2 + f_2^2\|y_{\vec{k}_h}(\vec{p}_h)\|^2) \\ &\quad= -\epsilon_{2,\iota}(\rho'_{k_h}(p_h))^{\mathrm{T}}\rho'_{k_h}(p_h) + \epsilon_{2,\iota}mf_1^2\|x_{k+1}(p) - e_{k+1}(p)\|^2\epsilon_{2,\iota}mf_2^2\|y_{\vec{k}_h}(\vec{p}_h)\|^2 \geqslant 0\end{aligned} \tag{30}$$

with $(\vec{k}_h,\vec{p}_h) \leqslant (k_h,p_h) \leqslant (k+1,p) < (k_{h+1},p_{h+1})$.

Combining the ET mechanism (7) and substituting inequalities (29) and (30) into (28) yields

$$\Delta V(k,p,\iota) \leqslant \zeta_1^{\mathrm{T}}(k,p)\Pi_{1,\iota}\zeta_1(k,p). \tag{31}$$

It follows from (17) that for any $\zeta_1^{\mathrm{T}}(k,p) \neq 0$, $k > \vec{k}_h$, and $p > \vec{p}_h$, we have $\Delta V(k,p,\iota) < 0$.

Case 2: $k = \vec{k}_h$ **and** $p > \vec{p}_h$**.**

By taking similar arguments in (28)–(31), for $k = \vec{k}_h$ and $p > \vec{p}_h$, Eq. (31) can be modified as

$$\Delta V(k,p,\iota) \leqslant \zeta_2^{\mathrm{T}}(k,p)\bar{\Pi}_{1,\iota}\zeta_2(k,p) < 0, \tag{32}$$

where $\zeta_2(k,p) \triangleq [\zeta_0^{\mathrm{T}}(k,p)\ \ \sum_{j=\vec{p}_h}^{p-1}(y_k(j+1) - y_{\vec{k}_h}(j))^{\mathrm{T}}]^{\mathrm{T}}$ and the second inequality is obtained by the inequalities in (18).

Case 3: $k > \vec{k}_h$ **and** $p = \vec{p}_h$**.**

Similarly, we have

$$\Delta V(k,p,\iota) \leqslant \zeta_3^{\mathrm{T}}(k,p)\bar{\Pi}_{1,\iota}\zeta_3(k,p) < 0, \tag{33}$$

where $\zeta_3(k,p) \triangleq [\zeta_0^{\mathrm{T}}(k,p) \quad \sum_{i=\vec{k}_h}^{k-1}(y_{i+1}(p)-y_i(\vec{p}_h))^{\mathrm{T}}]^{\mathrm{T}}$ and the second inequality is obtained by the inequalities in (18).

Case 4: $k=\vec{k}_h$ **and** $p=\vec{p}_h$**.**

From (16a), one has $y_k(p)=y_{\vec{k}_h}(\vec{p}_h)$. In the same way, we have

$$\Delta V(k,p,\iota) \leqslant \zeta_4^{\mathrm{T}}(k,p)\check{\Pi}_{1,\iota}\zeta_4(k,p) < 0, \tag{34}$$

where $\zeta_4(k,p) \triangleq [x_{k+1}^{\mathrm{T}}(p) \;\; e_{k+1}^{\mathrm{T}}(p) \;\; y_k^{\mathrm{T}}(p) \;\; u_{k+1}^{\mathrm{T}}(p-1) \;\; f^{\mathrm{T}}(x_{k+1}(p),y_k(p)) \;\; (\rho'_{k_h}(p_h))^{\mathrm{T}}]^{\mathrm{T}}$ and the second inequality is obtained by the inequalities in (19).

According to Definition 1, we conclude from (31), (32), (33), and (34) that the closed-loop system (15) is stable along the pass.

Remark 3. It is noted from Theorem 1 that there exist different sufficient conditions according to the location on the previous pass and the triggered location and pass, by which we can obtain different solutions. To be specific, different controller gains K_1 and K_2 will be obtained according to four different cases: $k>\vec{k}_h$ and $p>\vec{p}_h$; $k=\vec{k}_h$ and $p>\vec{p}_h$; $k>\vec{k}_h$ and $p=\vec{p}_h$; $k=\vec{k}_h$ and $p=\vec{p}_h$. This indicates that the designed sliding mode controller (11) can be regarded as a kind of switching-like controller, whose gains will switch according to the triggered location and pass. This characteristic is also reflected in the conditions of Theorems 2 and 3 and simulation results later.

Next, we analyze the reachability of sliding surface $s_{k+1}(p)=0$.

Theorem 2. Given parameter $\theta\in[0,1)$, if there exist matrices $P_{1,\iota}>0$, $P_{2,\iota}>0$, $P_{3,\iota}>0$, $Q_\iota>0$, $\Omega>0$, $Y_\iota=Y_\iota^{\mathrm{T}}$, G_1, G_2, K_1, K_2, and positive scalars $\epsilon_{1,\iota}$, $\epsilon_{2,\iota}$ satisfying (for $\iota,\bar{\iota}=1,2,\ldots,m$)

$$\Pi_\iota \triangleq \Pi_{1,\iota}+\Gamma_{4,\iota}^{\mathrm{T}}Q_{\bar{\iota}}\Gamma_{4,\iota}<0, \quad \text{for } k>\vec{k}_h \text{ and } p>\vec{p}_h, \tag{35}$$

$$\bar{\Pi}_\iota \triangleq \bar{\Pi}_{1,\iota}+\bar{\Gamma}_{4,\iota}^{\mathrm{T}}Q_{\bar{\iota}}\bar{\Gamma}_{4,\iota}<0, \quad \text{for } k=(>)\ \vec{k}_h \text{ and } p>(=)\ \vec{p}_h, \tag{36}$$

$$\check{\Pi}_\iota \triangleq \check{\Pi}_{1,\iota}+\check{\Gamma}_{4,\iota}^{\mathrm{T}}Q_{\bar{\iota}}\check{\Gamma}_{4,\iota}<0, \quad \text{for } k=\vec{k}_h \text{ and } p=\vec{p}_h, \tag{37}$$

where $\hat{\Gamma}_{4,\iota} \triangleq \sqrt{2}[\hat{A} \;\; -\hat{B}\Phi_\iota K_1 \;\; \hat{B}_0 \;\; \hat{B}\Phi_\iota K_2 \;\; \hat{B}(I-\Phi_\iota) \;\; B \;\; -\hat{B}\Phi_\iota]$, $\check{\Gamma}_{4,\iota} \triangleq \sqrt{2}[\hat{A} \;\; -\hat{B}\Phi_\iota K_1 \;\; \hat{B}_0+\hat{B}\Phi_\iota K_2 \;\; \hat{B}(I-\Phi_\iota) \;\; B \;\; -\hat{B}\Phi_\iota]$, $\Gamma_{4,\iota} \triangleq [\hat{\Gamma}_{4,\iota} \;\; 0 \;\; 0]$, $\hat{B} \triangleq G_1B+G_2D$, $\hat{B}_0 \triangleq G_1B_0+G_2D_0$, $\bar{\Gamma}_{4,\iota} \triangleq [\hat{\Gamma}_{4,\iota} \;\; 0]$, $\hat{A} \triangleq G_1A+G_1B\Phi_\iota K_1+G_2C+G_2D\Phi_\iota K_1$, other symbols are defined in Theorem 1, and the state trajectories of the closed-loop system (15) are driven into the following domain Θ around the surface $s_{k+1}(p)=0$:

$$\Theta \triangleq \left\{ s_{k+1}(p) \,\middle|\, \|s_{k+1}(p)\| \leqslant \sqrt{\frac{2\Delta}{\underline{Q}}}\|x_{k+1}(p)\| \right\} \tag{38}$$

with $\Delta \triangleq \overline{Q}\|G_1E\|^2\|H\|^2$, $\overline{Q} \triangleq \max\{\lambda_{\max}(Q_1),\ldots,\lambda_{\max}(Q_m)\}$, and $\underline{Q} \triangleq \min\{\lambda_{\min}(Q_1),\ldots,\lambda_{\min}(Q_m)\}$.

Proof. Select the Lyapunov functional as

$$W(k,p,\iota) = W_1(k+1,p,\iota)+V(k,p,\iota) \tag{39}$$

with $W_1(k+1,p,\iota) \triangleq s_{k+1}^{\mathrm{T}}(p)Q_\iota s_{k+1}(p)$ and $V(k,p,\iota)$ defined in Theorem 1.

We obtain from (3) and (15) that

$$\begin{aligned} s_{k+1}(p+1) =& (G_1\bar{A}+G_2C+G_2D\Phi_\iota K_1)x_{k+1}(p)-\hat{B}\Phi_\iota K_1e_{k+1}(p)+\hat{B}_0y_k(p)+\hat{B}\Phi_\iota K_2y_{\vec{k}_h}(\vec{p}_h) \\ &+Bf(x_{k+1}(p),y_k(p))-\hat{B}\Phi_\iota\rho_{k_h}(p_h)\mathrm{sign}(s_{k_h}(p_h))+\hat{B}(I-\Phi_\iota)u_{k+1}(p-1). \end{aligned} \tag{40}$$

According to the dynamics (40), one further has

$$\begin{aligned} \Delta W(k,p,\iota) &= \Delta V(k,p,\iota)+\Delta W(k,p,\iota) \\ &\leqslant \zeta^{\mathrm{T}}(k,p)\Pi\zeta(k,p)+2x_{k+1}^{\mathrm{T}}(p)\Delta A^{\mathrm{T}}(p)G_1^{\mathrm{T}}Q_{\bar{\iota}}G_1\Delta A(p)x_{k+1}(p)-s_{k+1}^{\mathrm{T}}(p)Q_\iota s_{k+1}(p), \end{aligned} \tag{41}$$

where $\zeta(k,p)=\zeta_1(k,p)$, $\Pi=\Pi_\iota$ for $k>\vec{k}_h$, $p>\vec{p}_h$; $\zeta(k,p)=\zeta_2(k,p)$, $\Pi=\bar{\Pi}_\iota$ for $k=\vec{k}_h$, $p>\vec{p}_h$; $\zeta(k,p)=\zeta_3(k,p)$, $\Pi=\bar{\Pi}_\iota$ for $k>\vec{k}_h$, $p=\vec{p}_h$; and $\zeta(k,p)=\zeta_4(k,p)$, $\Pi=\check{\Pi}_\iota$ for $k=\vec{k}_h$, $p=\vec{p}_h$.

It follows from (35)–(37) that

$$\Delta W(k,p,\iota)<2\lambda_{\max}(Q_{\bar{\iota}})\|G_1E\|^2\|H\|^2\|x_{k+1}(p)\|^2-\lambda_{\min}(Q_\iota)\|s_{k+1}^{\mathrm{T}}(p)\|^2. \tag{42}$$

Once $\|s_{k+1}(p)\|\geqslant\sqrt{\frac{2\Delta}{\underline{Q}}}\|x_{k+1}(p)\|$, i.e., the state trajectories are not within the domain Θ described by (38), we have $\Delta W(k,p,\iota)<0$ from (41). Consequently, the state trajectories of the system (15) are driven into Θ.

It is easy to prove that conditions (35)–(37) in Theorem 2 can ensure the stability and reachability simultaneously. The aforementioned conditions, however, are non-convex and not easy to solve. Therefore, the following theorem will further provide some solvable sufficient conditions.

Theorem 3. Given parameter $\theta\in[0,1)$, if there exist matrices $P_{1,\iota}>0$, $P_{2,\iota}>0$, $P_{3,\iota}>0$, $\bar{Q}_\iota>0$, $\Omega>0$, $Y_\iota=Y_\iota^{\mathrm{T}}$, G_1, G_2, K_1, K_2, and positive scalars $\epsilon_{1,\iota}$, $\epsilon_{2,\iota}$ satisfying (for $\iota=1,2,\ldots,m$)

$$\Xi_\iota\triangleq\begin{bmatrix}\Pi_{11,\iota}+\hat{H} & \Xi_{12,\iota} & 0 & \Xi_{14,\iota}\\ * & \Xi_{22,\bar{\iota}} & \Xi_{23,\iota} & \Xi_{24,\iota}\\ * & * & -\epsilon_0 I & 0\\ * & * & * & -I\end{bmatrix}<0,\quad\text{for } k>\vec{k}_h \text{ and } p>\vec{p}_h, \tag{43}$$

$$\bar{\Xi}_\iota\triangleq\begin{bmatrix}\bar{\Pi}_{11,\iota}+\bar{H} & \bar{\Xi}_{12,\iota} & 0 & \bar{\Xi}_{14,\iota}\\ * & \Xi_{22,\bar{\iota}} & \Xi_{23,\iota} & \Xi_{24,\iota}\\ * & * & -\epsilon_0 I & 0\\ * & * & * & -I\end{bmatrix}<0,\quad\text{for } k=(>)\ \vec{k}_h \text{ and } p>(=)\ \vec{p}_h, \tag{44}$$

$$\check{\Xi}_\iota\triangleq\begin{bmatrix}\check{\Pi}_{11,\iota}+\check{H} & \check{\Xi}_{12,\iota} & 0 & \check{\Xi}_{14,\iota}\\ * & \Xi_{22,\bar{\iota}} & \Xi_{23,\iota} & \Xi_{24,\iota}\\ * & * & -\epsilon_0 I & 0\\ * & * & * & -I\end{bmatrix}<0,\quad\text{for } k=\vec{k}_h \text{ and } p=\vec{p}_h, \tag{45}$$

where $\check{H}\triangleq\mathrm{diag}\{\epsilon_0H^{\mathrm{T}}H,0,0,0\}$, $\bar{H}\triangleq\mathrm{diag}\{\check{H},0,0\}$, $\hat{H}\triangleq\mathrm{diag}\{\bar{H},0\}$, $\Xi_{12,\iota}\triangleq[\Upsilon_{1,\iota}^{\mathrm{T}}\ \Upsilon_{2,\iota}^{\mathrm{T}}\ \Upsilon_{3,\iota}^{\mathrm{T}}\ \Upsilon_{4,\iota}^{\mathrm{T}}]$, $\bar{K}\triangleq[K_1^{\mathrm{T}}\ -K_1^{\mathrm{T}}\ 0\ K_2^{\mathrm{T}}\ 0\ 0\ 0]^{\mathrm{T}}$, $\bar{\Xi}_{12,\iota}\triangleq[\bar{\Upsilon}_{1,\iota}^{\mathrm{T}}\ \bar{\Upsilon}_{2,\iota}^{\mathrm{T}}\ \bar{\Upsilon}_{3,\iota}^{\mathrm{T}}\ \bar{\Upsilon}_{4,\iota}^{\mathrm{T}}]$, $\check{\Xi}_{12,\iota}\triangleq[\check{\Upsilon}_{1,\iota}^{\mathrm{T}}\ \check{\Upsilon}_{2,\iota}^{\mathrm{T}}\ \check{\Upsilon}_{3,\iota}^{\mathrm{T}}\ \check{\Upsilon}_{4,\iota}^{\mathrm{T}}]$, $\Xi_{22,\bar{\iota}}\triangleq\mathrm{diag}\{-P_{1,\bar{\iota}},-P_{2,\bar{\iota}},-P_{3,\bar{\iota}},-\bar{Q}_{\bar{\iota}}\}$, $\Xi_{14,\iota}\triangleq[\bar{K}\ 0\ 0]^{\mathrm{T}}$, $\Xi_{24,\iota}\triangleq[\Phi_\iota B^{\mathrm{T}}P_{1,\bar{\iota}}\ \Phi_\iota P_{2,\bar{\iota}}\ \Phi_\iota D^{\mathrm{T}}P_{3,\bar{\iota}}\ 0]^{\mathrm{T}}$, $\Xi_{23,\iota}\triangleq[E^{\mathrm{T}}P_{1,\bar{\iota}}\ 0\ 0\ 0]^{\mathrm{T}}$, $\bar{\Xi}_{14,\iota}\triangleq[\bar{K}\ 0]^{\mathrm{T}}$, $\check{\Xi}_{14,\iota}\triangleq[K_1^{\mathrm{T}}\ -K_1^{\mathrm{T}}\ K_2^{\mathrm{T}}\ 0\ 0\ 0]^{\mathrm{T}}$, $\hat{\Upsilon}_{1,\iota}\triangleq P_{1,\bar{\iota}}[A\ 0\ B_0\ 0\ B(I-\Phi_\iota)\ B\ -B\Phi_\iota]$, $\Upsilon_{q,\iota}\triangleq[\hat{\Upsilon}_{q,\iota}\ 0\ 0]$, $\hat{\Upsilon}_{2,\iota}\triangleq P_{2,\bar{\iota}}[0\ 0\ 0\ 0\ I-\Phi_\iota\ 0\ -\Phi_\iota]$, $\check{\Upsilon}_{2,\iota}\triangleq P_{2,\bar{\iota}}[0\ 0\ 0\ I-\Phi_\iota\ 0\ -\Phi_\iota]$, $\hat{\Upsilon}_{3,\iota}\triangleq P_{3,\bar{\iota}}[C\ 0\ D_0\ 0\ D(I-\Phi_\iota)\ 0\ -D\Phi_\iota]$, $\bar{Q}_{\bar{\iota}}\triangleq Q_{\bar{\iota}}^{-1}$, $\check{\Upsilon}_{1,\iota}\triangleq P_{1,\bar{\iota}}[A\ 0\ B_0\ B(I-\Phi_\iota)\ B\ -B\Phi_\iota]$, $\hat{\Upsilon}_{4,\iota}\triangleq\hat{\Gamma}_{4,\iota}$, $\check{\Upsilon}_{3,\iota}\triangleq P_{3,\bar{\iota}}[C\ 0\ D_0\ D(I-\Phi_\iota)\ 0\ -D\Phi_\iota]$, $\check{\Upsilon}_{4,\iota}\triangleq\check{\Gamma}_{4,\iota}$, $\bar{\Upsilon}_{q,\iota}\triangleq[\hat{\Upsilon}_{q,\iota}\ 0]$, $q=1,\ldots,4$, and other symbols are defined in Theorems 1 and 2, both the stability of the closed-loop system (15) and the reachability of the specified sliding surface are achieved simultaneously.

Proof. Inequality (43) is equivalent to

$$\Xi_{1,\iota}\triangleq\Xi_{2,\iota}+(M+N)^{\mathrm{T}}(M+N)+\epsilon_0^{-1}E_1E_1^{\mathrm{T}}+\epsilon_0H_1^{\mathrm{T}}H_1<0 \tag{46}$$

with $E_1\triangleq[0\ \Xi_{23,\iota}^{\mathrm{T}}]^{\mathrm{T}}$, $H_1\triangleq[\hat{H}\ 0]$, $M\triangleq[\Pi_{14,\iota}^{\mathrm{T}}\ 0]^{\mathrm{T}}$, $N\triangleq[0\ \Pi_{24,\iota}^{\mathrm{T}}]^{\mathrm{T}}$, and $\Xi_{2,\iota}\triangleq\left[\begin{smallmatrix}\Pi_{11,\iota} & \Xi_{12,\iota}^{\mathrm{T}}\\ * & \Xi_{22,\bar{\iota}}\end{smallmatrix}\right]$.

Based on the relations $M^{\mathrm{T}}N+N^{\mathrm{T}}M\leqslant(M^{\mathrm{T}}+N^{\mathrm{T}})(M+N)$ and $\Delta A(p)=E\Gamma(p)H$, we have

$$\Xi_{3,\iota}\leqslant\Xi_{1,\iota}<0 \tag{47}$$

with

$$\Xi_{3,\iota}\triangleq\begin{bmatrix}\Pi_{11,\iota} & \Gamma_{1,\iota}^{\mathrm{T}}P_{1,\bar{\iota}} & \Gamma_{2,\iota}^{\mathrm{T}}P_{2,\bar{\iota}} & \Gamma_{3,\iota}^{\mathrm{T}}P_{3,\bar{\iota}} & \Gamma_{4,\iota}^{\mathrm{T}}\\ * & -P_{1,\bar{\iota}} & 0 & 0 & 0\\ * & * & -P_{2,\bar{\iota}} & 0 & 0\\ * & * & * & -P_{3,\bar{\iota}} & 0\\ * & * & * & * & -\bar{Q}_{\bar{\iota}}\end{bmatrix}.$$

Pre- and post-multiplying the inequality (47) by the block-diagonal matrix $\mathrm{diag}\{I, P_{1,\bar{\iota}}^{-1}, P_{2,\bar{\iota}}^{-1}, P_{3,\bar{\iota}}^{-1}, I\}$, we have $\Pi_\iota < 0$; i.e., conditions (35) in Theorem 2 hold. Similarly, conditions (44) and (45) can guarantee conditions (36) and (37) in Theorem 2, respectively. Thus, both the stability and the reachability can be obtained simultaneously.

5 Application to metal rolling process

Metal rolling is an extremely common industrial process in which the workpiece is deformed between two counter-rotating rolls with parallel axes. Its essential feature is that the metal strip reaches a predetermined thickness through the repeated operation of a series of rollers, which is a typical repetitive process. In this section, the metal rolling process is applied to illustrate the proposed control scheme for discrete LRPs.

The linearized model of the metal rolling process proposed in [2] is made up of three separate roll pairs (see Figure 1 in [2]). A distinct rolling force regulates each roll. The metal strip can be rolled to a specific thickness by repeatedly reducing a set of rolls. Besides, as the metal strip passes through the rolls, an additional frictional force will be generated on the roller bearing, adjustment mechanism, and other parts of the rolling mill. This frictional force $\bar{f}_k(p)$ is the unknown function and connected with the actual roll gap thickness. Thus, the multi-roll rolling model in [2] is redescribed as

$$\begin{cases} \ddot{y}_{3\bar{k}+1}(t) + a_{01}y_{3\bar{k}+1}(t) + b_{21}\ddot{y}_{3\bar{k}}(t) + b_{01}y_{3\bar{k}}(t) = c_{01}(\bar{u}_{3\bar{k}+1}(t) + \bar{f}_{3\bar{k}+1}(t)), \\ \ddot{y}_{3\bar{k}+2}(t) + a_{01}y_{3\bar{k}+2}(t) + b_{21}\ddot{y}_{3\bar{k}+1}(t) + b_{01}y_{3\bar{k}+1}(t) = c_{01}(\bar{u}_{3\bar{k}+2}(t) + \bar{f}_{3\bar{k}+2}(t)), \\ \ddot{y}_{3\bar{k}+3}(t) + a_{01}y_{3\bar{k}+3}(t) + b_{21}\ddot{y}_{3\bar{k}+2}(t) + b_{01}y_{3\bar{k}+2}(t) = c_{01}(\bar{u}_{3\bar{k}+3}(t) + \bar{f}_{3\bar{k}+3}(t)) \end{cases} \tag{48}$$

for $t \in [0, N]$ and $\bar{k} \geqslant 0$, where $a_{0i} = \frac{\lambda_{1i}\lambda_2}{M_i(\lambda_{1i}+\lambda_2)}$, $b_{2i} = \frac{-\lambda_2}{\lambda_{1i}+\lambda_2}$, $b_{0i} = \frac{-\lambda_{1i}\lambda_2}{M_i(\lambda_{1i}+\lambda_2)}$, and $c_{0i} = \frac{-\lambda_{1i}}{M_i(\lambda_{1i}+\lambda_2)}$, $i = 1, 2, 3$.

Utilizing the difference $y_{3\bar{k}+i}(t) - y_{3\bar{k}+i}(t-\bar{T})$, $i = 1, 2, 3$ in the place of the differential $\dot{y}_{3\bar{k}+i}(t)$ and defining $t = p\bar{T}$ and the sampling period as $\bar{T}$, model (48) can be converted into model (1) with $A_p = A$ and the corresponding variables and parameters as in [2]. In particular, we consider the case that the model matrix A_p defined in (1) is not precisely known with $A_p = A + \Delta A(p)$, and

$$\Delta A(p) = \mathrm{diag}\{\Delta A_1(p), \Delta A_2(p), \Delta A_3(p)\},\ E = \mathrm{diag}\{E_1, E_2, E_3\},\ H = \mathrm{diag}\{H_1, H_1, H_1\},$$

$$\Delta A_i(p) = \frac{1}{1 + a_{0i}\bar{T}^2}\begin{bmatrix} 0 & 0.01\sin(p) \\ 0.05\sin(p) & 0 \end{bmatrix}, H_1 = \begin{bmatrix} 0.01 & 0 \\ 0 & 0.05 \end{bmatrix}, E_i = \begin{bmatrix} \frac{1}{1+a_{0i}\bar{T}^2} & 0 \\ 0 & \frac{1}{1+a_{0i}\bar{T}^2} \end{bmatrix},\quad i = 1, 2, 3.$$

Given the relevant parameters of the multi-roll metal rolling process as $\lambda_{11} = 40$ N/m, $\lambda_{12} = 60$ N/m, $\lambda_{13} = 80$ N/m, $\lambda_2 = 100$ N/m, $M_1 = 10$ kg, $M_2 = 20$ kg, $M_3 = 30$ kg, $\bar{T} = 0.8$, $f_1 = 0.15$, $f_2 = 0.1$, we design the SMC law (11) under the ET mechanism (7) with threshold $\theta = 0.1$ and RR protocol (12) in the C/A channel. By solving conditions (43)–(45) in Theorem 3, we obtain the following controller gains ($K_1 \triangleq [K_{11}\ K_{12}]$) according to the triggered location and pass:

$$K_{11} = \begin{bmatrix} 0.0065 & 0.0020 & 0.0201 \\ 0.0089 & -0.0108 & -0.0093 \\ -0.0093 & 0.0043 & -0.0150 \end{bmatrix},\ K_{12} = \begin{bmatrix} -0.0237 & -0.0241 & 0.0040 \\ -0.0204 & -0.0158 & 0.0212 \\ 0.0236 & 0.0224 & -0.0047 \end{bmatrix},$$
$$K_2 = 10^{-4} \times [-0.3566\ 0.2150\ 0.0907]^{\mathrm{T}}$$

for $k > \vec{k}_h$ and $p > \vec{p}_h$, and

$$K_{11} = \begin{bmatrix} 0.0065 & 0.0016 & 0.0185 \\ 0.0084 & -0.0096 & -0.0067 \\ -0.0071 & 0.0030 & -0.0124 \end{bmatrix},\ K_{12} = \begin{bmatrix} -0.0229 & -0.0235 & 0.0046 \\ -0.0201 & -0.0155 & 0.0191 \\ 0.0182 & 0.0175 & -0.0029 \end{bmatrix},$$
$$K_2 = 10^{-4} \times [-0.3698\ 0.2265\ 0.0991]^{\mathrm{T}}$$

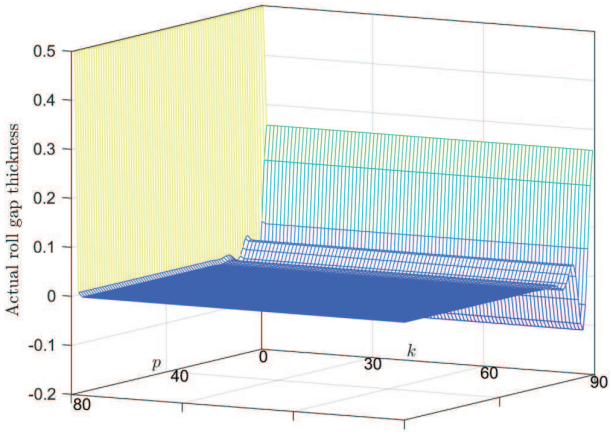

Figure 3 (Color online) Actual roll gap thickness.

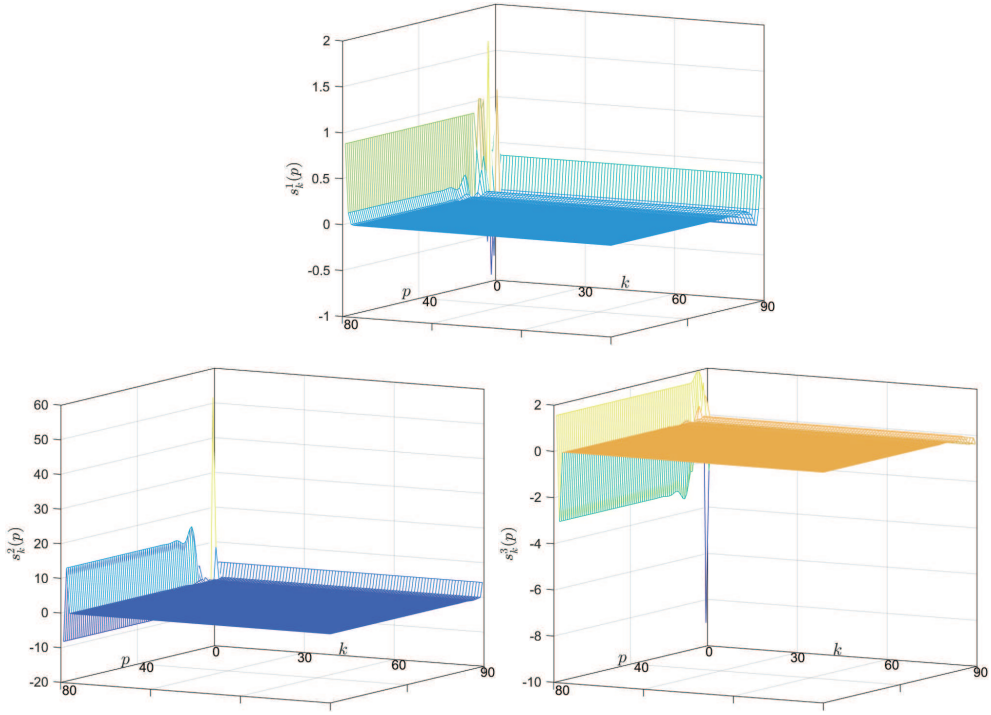

Figure 4 (Color online) Sliding variables.

for $k = \vec{k}_h$ and $p > \vec{p}_h$ or $k > \vec{k}_h$ and $p = \vec{p}_h$, and

$$K_{11} = 10^{-3} \times \begin{bmatrix} -0.0384 & 0.0312 & -0.0111 \\ -0.2328 & 0.1346 & -0.2984 \\ 0.1524 & -0.2964 & -0.6384 \end{bmatrix}, \quad K_{12} = 10^{-3} \times \begin{bmatrix} 0.0771 & 0.0711 & -0.0481 \\ 0.6112 & 0.5420 & -0.1912 \\ -0.1853 & -0.1185 & 0.6488 \end{bmatrix},$$

$$K_2 = [0.0099\ 0.0041\ 0.0022]^{\mathrm{T}}$$

for $k = \vec{k}_h$ and $p = \vec{p}_h$.

To prevent the control signals from chattering, the function $\mathrm{sign}(s_{k+1}(p))$ in the SMC law (11) is replaced by $s_{k+1}(p)/\|s_{k+1}(p)\| + 0.01$. Given the initial roll gap thickness $y_0(p) = 0.5$ for $p \in [0, 80]$ with the pass length N as 80, state variables $x_{k+1}(0) = [0.3\ 0.3]^{\mathrm{T}}$, simulation results are displayed in Figures 3–8. Figure 3 depicts the actual roll gap thickness under the influence of rolling force, and it is observed from Figure 3 that the process is stable along the roll. The sliding variables and input signals are shown in Figures 4 and 5, respectively. To compensate the influence of the RR protocol, it

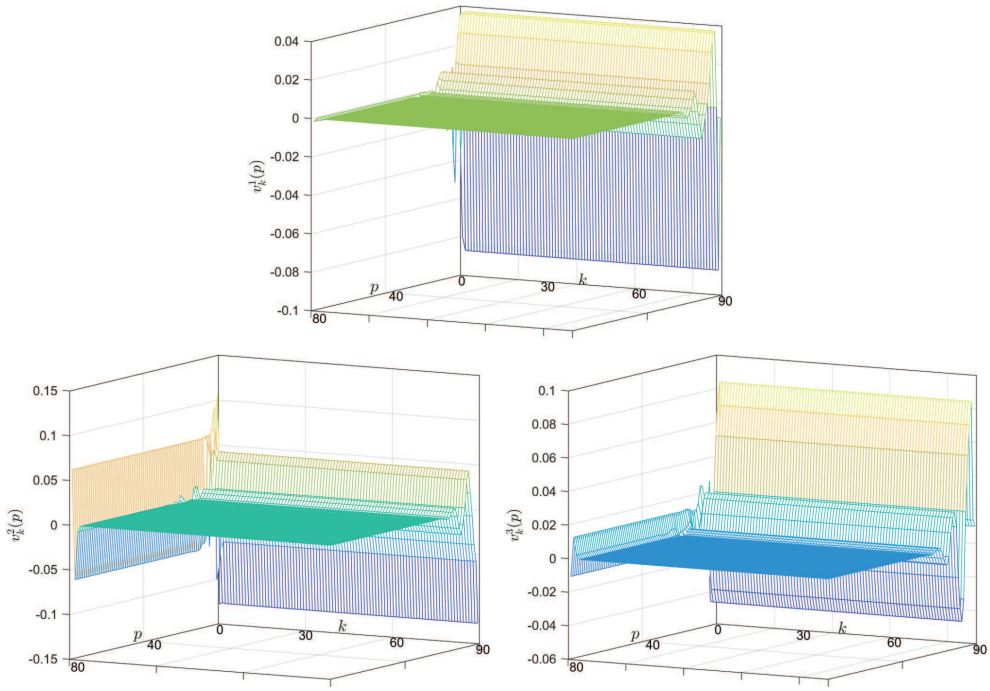

Figure 5 (Color online) Control signals.

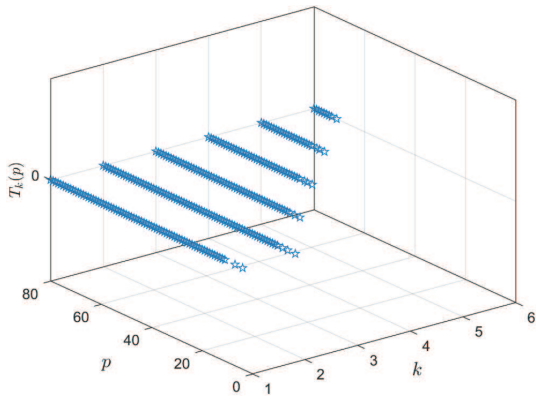

Figure 6 (Color online) Untransmitted points.

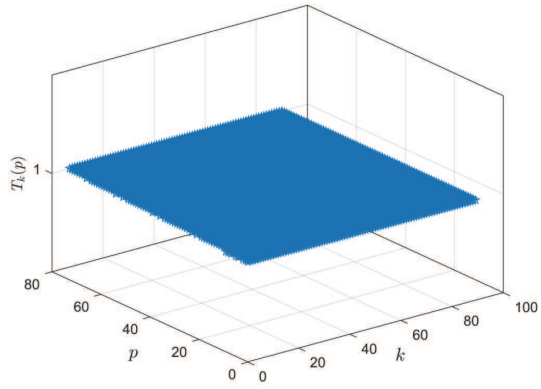

Figure 7 (Color online) Transmitted points.

is observed from Figures 6 and 7 that the triggering frequency is relatively high, in which the points satisfying $T_{k+1}(p) = 0$ and $T_{k+1}(p) = 1$ (in (8)) are plotted in Figures 6 and 7, respectively.

In addition, we compare different triggering thresholds and pass lengths with the simulation results shown in Table 1, in which the data transmission rate for the ET mechanism (7) is defined as (number of transmission points)/(80×90). It is noted from Table 1 that the transmission rate increases with decreasing triggering threshold or increasing pass length N.

Figure 8 shows the scheduling order of controller nodes under the updating rule (12), in which the blue points mean $\sigma_k(p) = 1$, the yellow ones mean $\sigma_k(p) = 2$, and the green ones mean $\sigma_k(p) = 3$. By fixing the pass k, it can be seen from Figure 8 that the color of points along the p direction changes in the order of blue, yellow, and green, which indicates that the tokens under the rule (12) are periodically arranged point-to-point along the pass direction and the rule (12) conforms to the evolution feature of LRPs.

6 Conclusion

This paper has addressed the design problem of sliding mode controller for LPRs under the limited network bandwidth. To reduce communication burdens, the ET mechanism has been presented in the

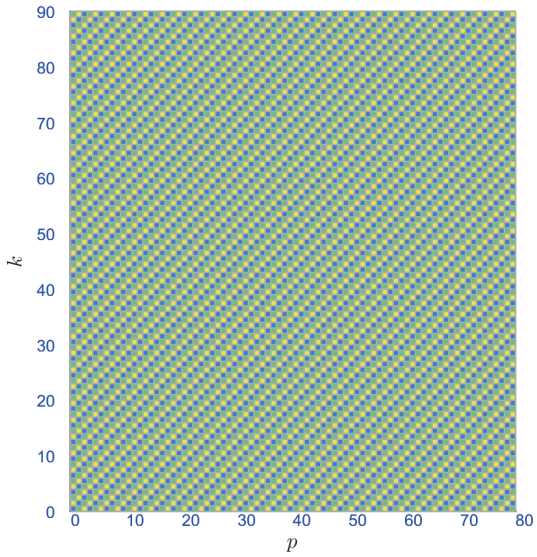

Figure 8 (Color online) Token under the updating rule (12).

Table 1 Results on different thresholds θ and pass lengths N

	$\theta = 0.0$	$\theta = 0.1$	$\theta = 0.2$	$\theta = 0.3$
		Number of transmission points		
N=80	7200	6919	6832	6824
N=60	4800	4526	4462	4454
N=30	2400	2126	2092	3984
		Transmission rate (%)		
N=80	100	96.1	94.88	94.77
N=60	100	94.29	92.95	92.79
N=30	100	88.58	87.16	86.83

S/C channel and the RR protocol has been adopted in the C/A channel, respectively. In particular, the triggered sequence and the order of the controller node accord with the evolution direction of LRPs. By employing the triggered states and pass profile signals, the switching-like SMC law has been designed and sufficient conditions have been given for ensuring stability along the pass and reachability. Further research might explore the impact of the pass length on other scheduling protocols including stochastic scheduling, weighted try-once discard protocol scheduling, and other dynamic scheduling.

Acknowledgements This work of Xinyu LV and Yugang NIU was supported in part by National Natural Science Foundation of China (Grant No. 62333006). This work of James LAM was supported by National Natural Science Foundation of China (Grant No. 62273286) and General Research Fund of Hong Kong (Grant No. 17203922).

References

1 Hladowski L, Galkowski K, Cai Z, et al. Experimentally supported 2D systems based iterative learning control law design for error convergence and performance. Control Eng Pract, 2010, 18: 339–348
2 Bochniak J, Gałkowski K, Rogers E, et al. Control law design for switched repetitive processes with a metal rolling example. In: Proceedings of IEEE International Conference on Control Applications, Singapore, 2007. 700–705
3 Rogers E, Gałkowski K, Owens D H. Control systems theory and applications for linear repetitive processes. In: Lecture Notes in Control and Information Sciences. Berlin: Springer-Verlag, 2007. 349: 23–34
4 Boudellioua M S, Galkowski K, Rogers E. Equivalent 2-D nonsingular Roesser models for discrete linear repetitive processes. Int J Control, 2018, 91: 2673–2681
5 Wu L, Lam J, Paszke W, et al. Control and filtering for discrete linear repetitive processes with $\mathcal{H}_\infty$ and $\updownarrow_2 - \updownarrow_\infty$ performance. Multidim Syst Sign Process, 2009, 20: 235–264
6 Li X, Lam J, Cheung K C. Generalized H_∞ model reduction for stable two-dimensional discrete systems. Multidim Syst Sign Process, 2016, 27: 359–382
7 Paszke W, Dabkowski P, Rogers E, et al. New results on strong practical stability and stabilization of discrete linear repetitive processes. Syst Control Lett, 2015, 77: 22–29
8 Wu L, Lam J. Hankel-type model reduction for linear repetitive processes: differential and discrete cases. Multidim Syst Sign Process, 2008, 19: 41–78
9 Ma H, Li H Y, Lu R Q, et al. Adaptive event-triggered control for a class of nonlinear systems with periodic disturbances. Sci China Inf Sci, 2020, 63: 150212

10 Sun Y, Shi P, Lim C C. Event-triggered sliding mode scaled consensus control for multi-agent systems. J Franklin Institute, 2022, 359: 981–998
11 Yao X Y, Park J H, Ding H F, et al. Coordination of a class of underactuated systems via sampled-data-based event-triggered schemes. IEEE Trans Syst Man Cybern Syst, 2022, 52: 2156–2166
12 Du X T, Zou L, Zhao Z Y, et al. Unknown-input-observer-based approach to dynamic event-triggered fault estimation for Markovian jump systems with time-varying delays. Sci China Inf Sci, 2022, 65: 132203
13 Li L, Yang R, Feng Z, et al. Event-triggered dissipative control for 2-D switched systems. Inf Sci, 2022, 589: 802–812
14 Lv X, Niu Y, Park J H, et al. Sliding mode control for 2D FMII systems: a bidirectional dynamic event-triggered strategy. Automatica, 2023, 147: 110727
15 Zhu K, Wang Z, Chen Y, et al. Event-triggered cost-guaranteed control for linear repetitive processes under probabilistic constraints. IEEE Trans Automat Contr, 2023, 68: 424–431
16 Yang R, Zheng W X, Yu Y. Event-triggered sliding mode control of discrete-time two-dimensional systems in Roesser model. Automatica, 2020, 114: 108813
17 Li D, Liang J, Wang F. Observer-based output feedback H_∞ control of two-dimensional systems with periodic scheduling protocol and redundant channels. IET Control Theor Appl, 2020, 14: 3713–3722
18 Li J, Niu Y, Song J. Sliding mode control design under multiple nodes round-robin-like protocol and packet length-dependent lossy network. Automatica, 2021, 134: 109942
19 Shi T, Zheng Y, Guan Y. Input-output finite-time control of Markov jump systems with round-robin protocol: an dynamic event-triggered approach. J Franklin Institute, 2022, 359: 3427–3443
20 Wang F, Wang Z, Liang J, et al. Resilient filtering for linear time-varying repetitive processes under uniform quantizations and round-robin protocols. IEEE Trans Circuits Syst I, 2018, 65: 2992–3004
21 Xu G, Xia Y, Zhai D H, et al. Adaptive prescribed performance terminal sliding mode attitude control for quadrotor under input saturation. IET Control Theor Appl, 2020, 14: 2473–2480
22 Xu J, Fridman E, Fridman L, et al. Static sliding mode control of systems with arbitrary relative degree by using artificial delay. IEEE Trans Automat Contr, 2020, 65: 5464–5471
23 Mei K Q, Ding S H. HOSM controller design with asymmetric output constraints. Sci China Inf Sci, 2022, 65: 189202
24 Zhao H, Zong G, Zhao X, et al. Hierarchical sliding-mode surface-based adaptive critic tracking control for nonlinear multi-player zero-sum games via generalized fuzzy hyperbolic models. IEEE Trans Fuzzy Syst, 2023, 31: 4010–4023
25 Su X, Liu X, Shi P, et al. Sliding mode control of discrete-time switched systems with repeated scalar nonlinearities. IEEE Trans Automat Contr, 2016, 62: 4604–4610
26 Qiu J, Ji W, Chadli M. A novel fuzzy output feedback dynamic sliding mode controller design for two-dimensional nonlinear systems. IEEE Trans Fuzzy Syst, 2020, 29: 2869–2877
27 Song J, Wang Y K, Niu Y. Dynamic event-triggered terminal sliding mode control under binary encoding: analysis and experimental validation. IEEE Trans Circuits Syst I, 2022, 69: 3772–3782
28 Wang T, Wang H, Xu N, et al. Sliding-mode surface-based decentralized event-triggered control of partially unknown interconnected nonlinear systems via reinforcement learning. Inf Sci, 2023, 641: 119070
29 Tian Y X, Li X, Dong B, et al. Event-based sliding mode control under denial-of-service attacks. Sci China Inf Sci, 2022, 65: 162203
30 Yang Y, Niu Y, Lam H K. Sliding-mode control for interval type-2 fuzzy systems: event-triggering WTOD scheme. IEEE Trans Cybern, 2023, 53: 3771–3781
31 Shang H, Zong G. Event-triggered sliding mode control under the Round-Robin protocol for networked switched systems. Nonlinear Dyn, 2020, 100: 2401–2413
32 Wu L, Gao H, Wang C. Quasi sliding mode control of differential linear repetitive processes with unknown input disturbance. IEEE Trans Ind Electron, 2010, 58: 3059–3068
33 Paszke W, Galkowski K, Rogers E, et al. $\mathcal{H}_\infty$ control of differential linear repetitive processes. IEEE Trans Circuits Syst II, 2006, 53: 39–44